International Journal of Integrated Engineering – Special Issue on Electrical Electronic Engineering
Vol. 9 No. 4 (2017) p. 93-102

Optimal Two-Degree-of-Freedom Control for Precise Positioning of a Piezo-Actuated Stage

Marwan Nafea[1], Colin Schlosser[2], Suhail Kazi[3], Zaharuddin Mohamed[1], Mohamed Sultan Mohamed Ali[1,*]

[1]Faculty of Electrical Engineering
Universiti Teknologi Malaysia, 81310 Skudai, Johor, Malaysia.
[2]British Columbia Cancer Research Centre
600 West 10th Avenue, Vancouver, BC V5Z 4E6, Canada.
[3]Faculty of Engineering
Islamic University of Madinah, Al Jamiah, 107 Medina, Saudi Arabia.

Abstract: Microelectromechanical systems (MEMS) based positioning stages are composed of a piezoelectric actuator (PEA) and a positioning mechanism. Hysteresis is one of the major factors that limit the positional accuracy of piezo-actuated stages. This paper presents a novel method for designing a two-degree-of-freedom (2DOF) controller for precise positioning of a MEMS-based piezo-actuated stage, where Bouc-Wen hysteresis model is used to represent the hysteresis behavior of the PEA. A Luenberger observer-based feed-forward controller is designed, and then integrated with a Particle Swarm Optimization (PSO)-based Proportional-Integral-Derivative (PID) controller to form a 2DOF controller. Optimal PID gains are obtained based on a new fitness function proposed to reduce the displacement error and achieve a fast response time. The results show that using the proposed 2DOF controller reduces the error to be in the range of 0.03 – 1.31% of the maximum displacement when the system is operated in the range of 1 – 50 Hz.

Keywords: Bouc-Wen hysteresis model, two-degree-of-freedom control, microelectromechanical systems (MEMS), piezoelectric actuator (PEA), piezo-actuated stage

1. Introduction

Microelectromechanical systems (MEMS) based positioning stages have been vastly applied in numerous applications, including scanning tunneling microscopy, atomic force microscopy, optical cross connects, and parallel-probe-based data-storage systems [1]. Various MEMS-based positioning stages that use different actuation principles and mechanical structures have been reported. Such actuation principles include electrostatic actuators, electromagnetic actuators, electrothermal actuators, shape-memory-alloy actuators, and piezoelectric actuators (PEAs) [2]. Among these actuation principles, PEAs have been widely utilized in such stages due to their special characteristics such as high resolution in the nanometer range, large bandwidth, fast response, and high stiffness [3]. A piezoelectric stack actuator is built by assembling piezoelectric wafers and electrodes so that the piezoelectric wafers are connected mechanically in series while being connected electrically in parallel, as illustrated in Fig. 1. The actuator elongates or contracts when applying a positive or a negative voltage on its electrodes. This movement is caused by the realignment of the crystalline polarization of the piezoelectric ceramic material [4].

PEAs main shortcomings are the nonlinearity caused by creep phenomenon, high-frequency vibrations, and hysteresis [5, 6]. Creep is a slow drift in the position that occurs after the desired motion when a constant input is applied to the PEA. This phenomenon is often represented by a nonlinear logarithmic model of time and input voltage [7], or by a linear dynamic model [8]. On

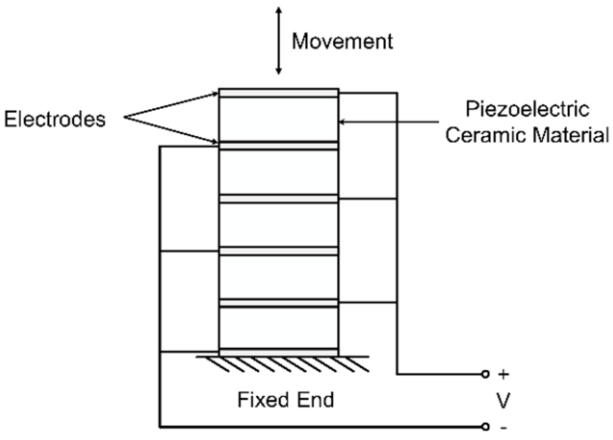

Fig. 1 Construction of a piezoelectric stack actuator.

*Corresponding author: sultan_ali@fke.utm.my

the other hand, unwanted vibrations occur when a PEA is operated at frequencies close to its first resonant frequency. This limits the operating frequencies of the PEA to less than 1% to 10% of the first resonant frequency [8]. These vibrations are generally modelled and compensated based on the known dynamics of the PEA [9]. While the hysteresis causes serious non-linear effects on the motion of PEAs, the non-linear effects of creep and near-resonant vibrations are relatively small. The nonlinear effect between the applied voltage and generated displacement causes difficulties in controlling the displacement of the actuator. In order to address these difficulties, an accurate modeling of hysteresis behavior should be implemented before designing a controller for hysteresis compensation. Many models have been developed to this end. These models can be classified into physical models and mathematical models. Physical models are derived based on the mechanism of PEA hysteresis, and they are often complicated; whereas mathematical models can be classified into static models and dynamic models. Preisach model, Prandtl-Ishlinskii model, and the polynomial model are considered as static hysteresis models, while Bouc-Wen model, Duhem model, and Maxwell slip model are considered as dynamic hysteresis models [10]. Dynamic hysteresis models are reported to be more accurately represent the nonlinear hysteresis behavior of PEAs, and Bouc-Wen hysteresis model is considered as a simple model with least number of parameters. Furthermore, it is reported to provide a great ability to handle any functional nonlinearity and has a high ability to model non-symmetrical hysteresis loops [11]. Despite the existence of such models, the tracking performance of PEAs still suffers from the effects of hysteresis.

Feedforward control can potentially enhance the output tracking performance in piezo-actuated systems. This can be done by utilizing feedforward inverse compensation, which inverts the mathematical model of the hysteresis to determine the hysteresis compensating input. Hysteresis inversion is suitable in low-frequency operations since creep in the actuator can be corrected using feedback control, and vibrations are negligible at low frequencies [8]. To overcome the complexity and inaccuracy that occur when applying the hysteresis inversion, especially when the system has asymmetric hysteresis loops behavior, a hysteresis observer is utilized to estimate the hysteresis effect [5]. However, modeling uncertainties and external disturbance usually exist in the system. Thus, a feedback controller is needed to enhance the robustness of the systems and to improve the tracking performance [12]. The use of integral controllers gives the advantage of providing high gain feedback at low frequencies, which overcomes creep and hysteresis effects in actuation. This makes traditional Proportional-Integral-Derivative (PID) feedback controllers suitable to control piezo-actuated stages [13]. Recently, research has gone into the automated tuning of the parameters of PID controllers, such as Particle Swarm Optimization (PSO), which finds the optimal solution for PID gains using a population of particles based on a designed fitness function [14]. PSO is a derivation-free method that does not use too many parameters, which makes it easy to be implemented to solve various optimization problems. In addition, this method produces robust solutions that are highly sensitive towards the parameters and objective functions, while being less dependent on the initial values. Furthermore, due to the single-directional information of particles, where each particle remembers its past position, it has a good global searching ability and very quick convergence [15].

Two-degree-of-freedom (2DOF) control methods that combine feedforward and feedback control can improve the tracking performance and reduce errors caused by nonlinearities, which makes this method sufficient when controlling PEAs in high-precision positioning applications. Such methods include the use of a Proportional-Integral (PI) feedback control associated with a feedforward compensating based on the hysteresis observer [5], a combination of a model-based feedforward controller and a PID feedback controller [16], and a 2DOF derivative/repetitive control [17]. Although these methods show promising results, the tracking error is still considerably large, especially when precise positioning system is required.

In this paper, a 2DOF control approach is designed and presented for precise positioning of piezo-actuated stages. This approach combines a feedforward controller based on Luenberger observer and a PSO-based PID feedback controller. Bouc-Wen hysteresis model is used to describe the hysteresis behavior of the PEA. A Luenberger observer is utilized to estimate the hysteresis nonlinearity, since this observer has an easy structure, and it is easy to implement. The parameters of the PID feedback controller are tuned based on a proposed PSO fitness function to achieve satisfactory time response specifications. The performance of the controller is evaluated in terms of time response specifications, error as compared to the desired response and capability in reducing the hysteresis effect.

2. Methodology

2.1 Modeling The Piezo-Actuated Stage

The model of the piezo-actuated stage presented in this section is shown in Fig. 2. The model is a moving stage driven by a piezoelectric stack actuator, where one end is fixed and the other is sliding horizontally. By

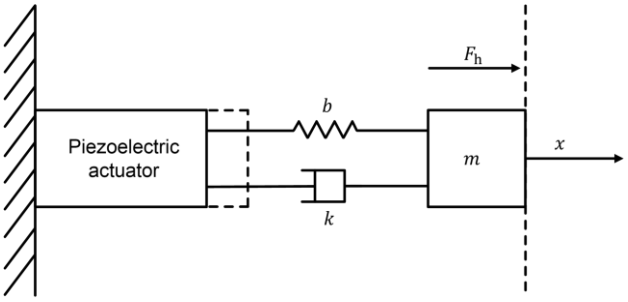

Fig. 2 Schematic diagram of the piezo-actuated stage.

assuming a high generated force by the piezoelectric stack actuator compared to the frictional force, the piezoelectric stack actuator is regarded as a force generator. The Bouc-Wen hysteresis model is utilized to model the hysteresis behavior of the piezoelectric stack actuator.

Using Newton Laws and considering the PEA as a mass-spring-damper system, Bouc-Wen hysteresis model of the piezo-actuated stage can be stated as follows:

$$m\ddot{x} + b\dot{x} + kx = F_h = k(du - h) + F_{ext} \quad (1)$$

$$\dot{h} = \alpha d\dot{u} - \beta|\dot{u}|h - \gamma\dot{u}|h| \quad (2)$$

where x is the displacement of the PEA, h is the hysteresis nonlinear term, and $\dot{x}$, $\ddot{x}$ and $\dot{h}$ are the derivatives of x and h, respectively. m, b and k are the mass, damper coefficient and stiffness factor of the whole positioning mechanism combined together, respectively. u is the applied voltage, F_{h} is the exciting force that generated by the piezoelectric ceramic, d is the piezoelectric material constant, F_{ext} is the external force applied by the load, while α, β and γ are parameters that control the shape and the amplitude of the hysteresis loop, where $0 < \alpha < 1$ [18]. The differential equations of the system can be represented in state-space form as:

$$\begin{bmatrix}\dot{x_1}\\ \dot{x_2}\\ \dot{x_3}\end{bmatrix} = \begin{bmatrix}0 & 1 & 0\\ -\frac{k}{m} & -\frac{b}{m} & -\frac{k}{m}\\ 0 & 0 & 0\end{bmatrix}\begin{bmatrix}x_1\\ x_2\\ x_3\end{bmatrix} + \begin{bmatrix}0 & 0\\ \frac{kd}{m} & 0\\ 0 & \alpha d\end{bmatrix}\begin{bmatrix}u_1\\ u_2\end{bmatrix} + |u_2|\begin{bmatrix}0 & 0 & 0\\ 0 & 0 & 0\\ 0 & 0 & -\beta\end{bmatrix}\begin{bmatrix}x_1\\ x_2\\ x_3\end{bmatrix} + u_2\begin{bmatrix}0 & 0 & 0\\ 0 & 0 & 0\\ 0 & 0 & -\gamma\end{bmatrix}\begin{bmatrix}x_1\\ x_2\\ x_3\end{bmatrix} \quad (3)$$

$$y = \begin{bmatrix}1 & 0 & 0\end{bmatrix}\begin{bmatrix}x_1\\ x_2\\ x_3\end{bmatrix} \quad (4)$$

where the states represent $x_1 = x$, $x_2 = \dot{x}_1 = \dot{x}$ and $x_3 = h$; the input represent $u_1 = u$ and $u_2 = \dot{u}$. Equations (3) and (4) can be represented in matrix form as:

$$\dot{x} = Ax + Bu + |u_2|Gx + u_2H|x| \quad (5)$$

$$y = Cx \quad (6)$$

2.2 Controller Design

2.2.1 Luenberger Observer-Based Feedforward Controller Design

Designing the feedforward controller for the piezo-actuated system requires an observer to estimate the hysteresis state. Furthermore, the problem of the velocity measurement can also be solved using the hysteresis observer to estimate the velocity of the positioning system. This will offer the opportunity to omit the velocity sensors, and thus reduce the cost and eliminate measurement noise [5]. A Luenberger observer [19] is utilized to observe the hysteresis of the piezo-actuated system since this observer has an easy structure and it is easy to implement. A block diagram of the Luenberger observer-based feedforward controller for the piezo-actuated system is shown in Fig. 3(a).

The Luenberger observer representation for this system is as follows:

$$\dot{\hat{x}} = A\hat{x} + Bu + |u_2|G\hat{x} + u_2H|\hat{x}| + L(y - \hat{y}) \quad (7)$$

$$\hat{y} = C\hat{x} \quad (8)$$

where $\hat{x}$ is the estimated state vector, $\hat{y}$ is the estimated output, and the observer gain, L should be chosen such that $A - LC$ is stable [19]. The output of the Luenberger observer is then combined with the original reference signal, x_{r}, to form a feedforward controller to compensate the hysteresis nonlinearity.

2.2.2 2DOF Controller Design

The 2DOF controller is designed by combining the feedforward controller with the feedback controller as shown in Fig. 3(b). In order to design the PID controller, the proportional gain, K_{P}, the integral gain, K_{I}, and the derivative gain, K_{D}, are tuned to eliminate the overshoot and to minimize the rise time, settling time and steady-state error.

As the PEA is highly nonlinear, in this work, PID gains are tuned using the PSO algorithm [15], which finds the optimal solution using a population of particles. Each position in a d-dimensional search space is a possible solution of the problem, and every particle is considered as a point in the search space, where x and v denote the position and the corresponding velocity of that particle, respectively. Thus, the i-th particle is represented as x_i =

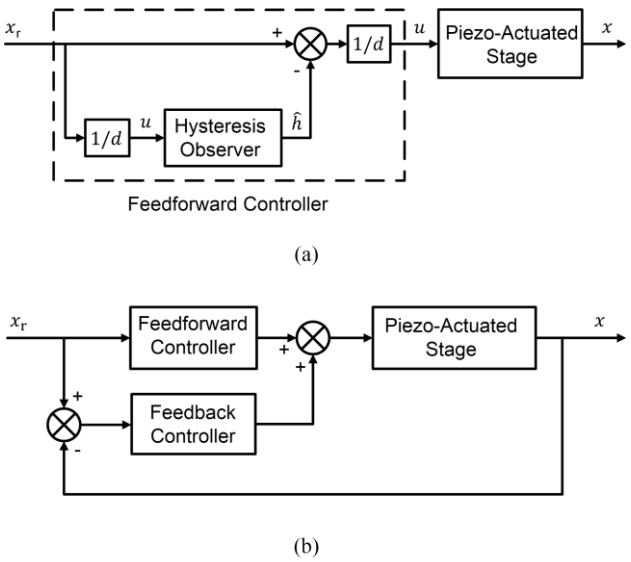

Fig. 3 A block diagram of the proposed structure: (a) Luenberger observer-based feedforward controller (b); The 2DOF controller structure.

$(x_{i,1}, x_{i,2}, \ldots, x_{i,d})$, and the velocity of the particle i is represented as $v_i = (v_{i,1}, v_{i,2}, \ldots, v_{i,d})$. The best previous position that gives the best fitness value of the i-th particle is recorded and expressed as $pbest_i = (pbest_{i,1}, pbest_{i,2}, \ldots, pbest_{i,d})$, while the index of the best particle of all particles in the population is donated by $gbest_d$. Then, the particles are manipulated according to the following equations [20]:

$$v_{i,d}(t+1) = w.v_{i,d}(t) + c_1 * r_1 * \left(pbest_{i,d}(t) - x_{i,d}(t)\right) + c_2 * r_2 * \left(gbest_d(t) - x_{i,d}(t)\right) \quad (9)$$

$$x_{i,d}(t+1) = x_{i,d}(t) + v_{i,d}(t+1) \quad (10)$$

where

i	1, 2, …, n
d	1, 2, …, m
t	index of iterations (generations);
n	number of particles in a group;
m	number of members in a particle (dimension of the problem);
$v_{i,d}(t)$	velocity of a particle i at iteration t, and $v_d^{\min} \le v_{i,d} \le v_d^{\max}$;
w	intertie weight factor;
c_1, c_2	acceleration factor;
r_1, r_2	random numbers in the range of [0, 1];
$x_{i,d}(t)$	position of a particle i at iteration t, and $x_d^{\min} \le x_{i,d} \le x_d^{\max}$;
$pbest_i$	$pbest$ of particle i;
$gbest$	$gbest$ of the group.

In the definitions above, the minimum and maximum values of velocity are restricted between two constraints, $v_d^{\min}$ and $v_d^{\max}$, respectively. The parameter $v_d^{\max}$ specifies the resolution of search in the regions between the current position and the target position. Too high values of $v_d^{\max}$ might lead the particles to pass good solution. On the other hand, too small values of $v_d^{\max}$ might limit exploring new good solutions beyond locally good regions, or even trapped in local optima [21]. Thus, the value of $v_d^{\max}$ is often set to be 50% of the dynamic range of the variable on each dimension [20]. The parameters $x_d^{\min}$ and $x_d^{\max}$ are the minimum and maximum boundaries of the position of particles on each dimension. These parameters are set to be in the feasible range of solution of on each dimension. The constants c_1 and c_2 are the cognitive acceleration factor and the social acceleration factor, respectively. These constants scale the influence of $pbest$ and $gbest$ on the solution. Low values allow particles to explore new regions far from the target before being pulled back, while high values lead particles to move suddenly toward target regions. Thus, these constants are often set to be 2.0 to balance between local and global search, since its average makes the weights for cognitive and social parts equal to 1.0 [21]. Furthermore, to balance the trade-off between local and global exploration for different problems, the inertia weight w is usually decreased linearly from 0.9 to 0.4 during the run as follows [22]:

$$\omega = \frac{\omega_{max} - \omega_{min}}{iter_{max}} \times iter \quad (11)$$

where $w_{\max}$ and $w_{\min}$ are the maximum and the minimum values of the inertia weight, respectively, $iter_{\max}$ is the maximum number of iterations, and $iter$ is the current number of iteration [20].

By applying the PSO equations on the PID tuning problem, the position of the particles represents the gains of the PID controller, which means that $d = 3$ and $x = [K_P, K_I, K_D]$. The solution of the PSO is based on the performance index, which is a quantitative measure to determine the performance of the designed PID controller. In this paper, a new fitness function is proposed to evaluate the performance of the PID controller in the time domain, including overshoot (M_P), steady-state error (E_{ss}), rise time (t_r) and settling time (t_s). Thus, the fitness function, F is defined as follows:

$$F = 10^{\delta} \cdot (M_P + E_{ss}) + 10^{-\delta} \cdot (t_r - t_s) \quad (12)$$

where δ is the weighting factor. The fitness function can be adjusted to meet the designer requirements using the value of δ. Increasing the value of δ has a positive effect on the overshoot and steady-state error while decreasing it has a positive effect on the rise time and settling time. Selecting the suitable value of δ is based on the previous knowledge of the dynamic performance of the system. The proposed fitness function provides a tunable trade-off between the performance criteria in the time domain. The search steps of the proposed PSO-based PID controller are as follows:

Step 1: Specify the lower and upper boundaries of the controller parameters, and initialize the particles with random positions, velocities, $pbests$ and $gbest$.

Step 2: Calculate the fitness function value of each particle in the population using Equation (12).

Step 3: Compare fitness function value of each particle with its $pbest$. If the current value is smaller than $pbest$, then set $pbest$ value to be equal to the current value, and the $pbest$ location to be equal to the current position in the d-dimensional search space.

Step 4: Compare fitness function value with the overall previous best. If the current value is smaller than $gbest$, then set $gbest$ to the current value and position.

Step 5: Modify the velocity (v) of each particle (t) according to Equation (9), where w is calculated according to Equation (12).

Step 6: If $v_{i,d}(t+1) \le v_d^{\min}$, then $v_{i,d}(t+1) = v_d^{\min}$; If $v_{i,d}(t+1) \ge v_d^{\max}$, then $v_{i,d}(t+1) = v_d^{\max}$.

Step 7: Modify the position (x) of each particle (t) according to Equation (10).

Step 8: If $x_{i,d}(t+1) \le x_d^{\min}$, then $x_{i,d}(t+1) = x_d^{\min}$; If $x_{i,d}(t+1) \ge x_d^{\max}$, then $x_{i,d}(t+1) = x_d^{\max}$.

Step 9: If the number of iterations reaches the maximum then, go to *Step 10*. Otherwise, go to *Step 2*.

Step 10: The particle that generates the latest $gbest$ is the optimal controller parameter.

3. Results and Discussion

3.1 Dynamic Behavior and Feedforward Control

Studying the displacement of the piezo-actuated stage requires analyzing the dynamic behavior of the whole system under study. This is done by utilizing the Bouc-Wen hysteresis model that relates the displacement of the piezo-actuated system to the applied voltage using Equations (3) and (4). In this study, the values of the parameters of the system are taken from a previous work [23], as given in Table 1.

A triangular input voltage with an amplitude of 80 V and a frequency of 1 Hz is used to test the performance of the open-loop system. The input voltage is multiplied by the piezoelectric material constant, d, to give the value of the corresponding reference displacement signal. A feedforward controller is then utilized to enhance the output tracking performance of the piezo-actuated system. Thus, a Luenberger observer-based feedforward controller structure, shown in Fig. 3(a), is utilized to track the reference trajectory applied in the open-loop system. Fig. 4(a) shows the open-loop and the feedforward control trajectory responses of the system as compared to the reference signal. It can be seen that open-loop the displacement evinces a distortion on both rising and falling slopes, which indicates a hysteretic nonlinear relationship between the input voltage and the displacement of the PEA [4]. In addition, Fig. 4(b) demonstrates the resultant error between the reference signal and both of the open-loop displacement and the feedforward control trajectory tracking responses. The results show that the error of the open-loop response varies in the range of -7.43 to 7.50 µm, where the negative sign refers to the direction of movement. Furthermore, it can be seen that the tracking error has been reduced to be in the range of -3.49 and 3.50 µm, when using the feedforward controller, indicating a reduction in the error by 53.31% as compared to the open-loop error. The resultant error in both cases is caused by hysteresis that occurs between the input voltage and the displacement. This phenomenon is demonstrated in Fig. 4(c), which shows the nonlinear hysteresis relationships between the input voltage and the displacement of both of the open-loop system and feedforward-controlled system. The hysteresis is caused by the crystalline polarization effect and molecular friction. The displacement generated by the piezoelectric actuator depends on the applied electric field and the piezoelectric material constant, which is related to the remnant polarization that is affected by the electric field applied on the piezoelectric material. The current value of the hysteresis curve depends on the previous value of the input voltage since the piezoelectric materials remain

Table 1 Values of the system parameters

Parameter	Value	Parameter	Value
m	2.17 kg	α	0.38
b	4378.67 Ns/m	β	0.0335
k	3×10^{5} N/m	γ	0.0295
d	9.013×10^{-7} m/V	F_{ext}	0 N

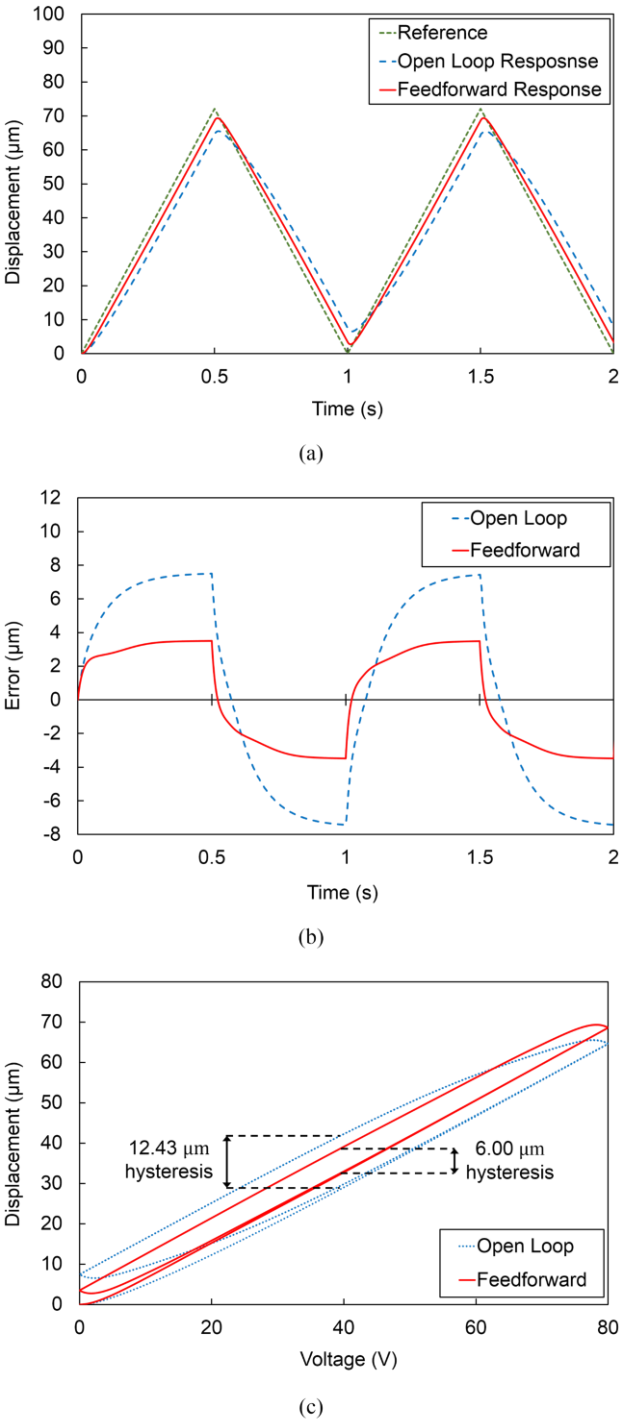

Fig. 4 Open-loop and feedforward control results: (a) Trajectory responses compared with the reference signal; (b) Trajectory tracking errors; (c) Hysteresis relationships.

Table 2 Comparison of the performance criteria in time domain

δ	P	K_P	K_I	K_D	t_r (ms)	t_s (ms)	M_P(%)	E_{SS} (μm)
1	20	181.5200	38.3183	0.0526	0.7640	0.9930	0.0122	0.0197
	30	188.4621	38.6425	0.0537	0.7480	0.9690	0.0195	0.0206
2	20	189.7459	46.4110	0.0542	0.7500	0.9740	0.0114	0.0179
	30	197.3215	47.8519	0.0560	0.7430	0.9680	0.0000	0.0182
3	20	196.9657	48.7367	0.0559	0.7430	0.9680	0.0047	0.0181
	30	197.3495	47.7607	0.0560	0.7430	0.9680	0.0000	0.0182

Table 3 Comparison of the convergence characteristics

δ	P	*Min. (*Best*)*	*Max. (*Worst*)*	*ΔE (max-min)*	Average	*SD*
1	20	2.2223×10^{-5}	4.1558×10^{-5}	1.9335×10^{-5}	2.2696×10^{-5}	5.4503×10^{-6}
	30	2.2223×10^{-5}	3.8815×10^{-5}	1.6591×10^{-5}	2.3352×10^{-5}	3.5506×10^{-6}
2	20	4.0380×10^{-6}	8.8984×10^{-6}	4.8604×10^{-6}	4.3405×10^{-6}	1.0525×10^{-6}
	30	4.0380×10^{-6}	4.1000×10^{-6}	6.1992×10^{-7}	4.2123×10^{-6}	1.5614×10^{-8}
3	20	1.8170×10^{-5}	2.0809×10^{-5}	2.6390×10^{-6}	1.8393×10^{-5}	5.9274×10^{-7}
	30	1.8170×10^{-5}	2.2361×10^{-5}	4.1911×10^{-6}	1.9848×10^{-5}	9.1281×10^{-7}

magnetized after the external magnetic field is removed. As indicated in Fig. 4(c), the initial ascending displacement curves start from the origin, but they do not return to the origin even if the applied voltage is back to zero. This is caused by the polarization and elongation that occurs in the piezoelectric material under positive voltages, which cannot be completely retrieved even if the input voltage returns to zero [4]. The figure demonstrates that the hysteresis value at 50% of the voltage swing (40 V) has decreased from 13.43 to 6.00 μm, indicating a reduction in the hysteresis by 51.73% when using the feedforward controller. However, this response lacks the robustness and it is sensitive to the parameters uncertainties and modeling errors. These drawbacks can be eliminated using feedback control combined with feedforward to form a 2DOF control structure since pure feedback control is not suitable for high-speed tracking control [16, 24].

3.2 2DOF Tracking Control

In order to achieve a highly precise positioning while actuating the piezo-actuated stage, a 2DOF control structure that can improve the tracking performance and reduce errors caused by nonlinearities is utilized. The 2DOF control structure consists of the Luenberger observer-based feedforward controller and a PSO-based PID feedback controller, as illustrated in Fig. 3(b).

The fitness function in Equation (12) is used to tune the gains of the PSO-based PID feedback controller while it is integrated with the Luenberger-observer-based feedforward controller. The minimum and maximum boundaries of the three parameters of the PID controller are selected to be in the feasible range of the solution, where K_P, K_I and K_D are set in the ranges of 0 – 300, 0 – 80, and 0 – 2, respectively. The PSO parameters that are used to tune the PID controller are set to be as discussed in Section 3.2, where the number of generations is 300 (the members of each particle are K_P, K_I and K_D) and the limit of change in velocity of each particle is as follows:

$$v_d^{\max} = x_d^{\max}/2 \tag{13}$$

The performance of the 2DOF controller is implemented in MATLAB/Simulink using a 4th-order Runge-Kutta method with the fixed step size of 0.0001 s. A step input with an amplitude of 80 V is used to test the time domain performance criteria (rise time, settling time, overshoot and steady-state error), while six simulation examples are carried out to evaluate the performance of the 2DOF controller based on those criteria. Each two examples are set to have the same value of the weighting factor δ while having different population sizes (P). In the first two examples, δ is set to be 1 to neutralize between the overshoot and steady-state error on one side, and the rise time and settling time on the other, as described earlier in Equation (12). Then, the value of δ is increased to observe its effect on the tuning process. The population size is set to be 20 or 30 in the simulation examples to observe its effect on the accuracy and speed of the searching process. The values of the population size are selected based on previous experience. Additionally, 20 trials of each simulation example are performed with different random numbers to study the variation of their evaluation values. The simulation results of these examples are summarized in Table 2.

As indicated in Table 2, the fourth simulation example with a weighting factor δ of 2, and a population size of 30 gives the fastest time response and the lowest overshoot and steady-state error, which make it the best solution. In addition, Table 3 presents a comparison between the evaluation values of each example and provides an observation of the variation between those evaluation values. It is clear that the fourth simulation example has the least difference between its minimum and maximum evaluation value, and has the lowest variation from its average (lowest standard deviation (SD)).

Further observations of the values of the PID gains in each generation (iteration) of the fourth example show

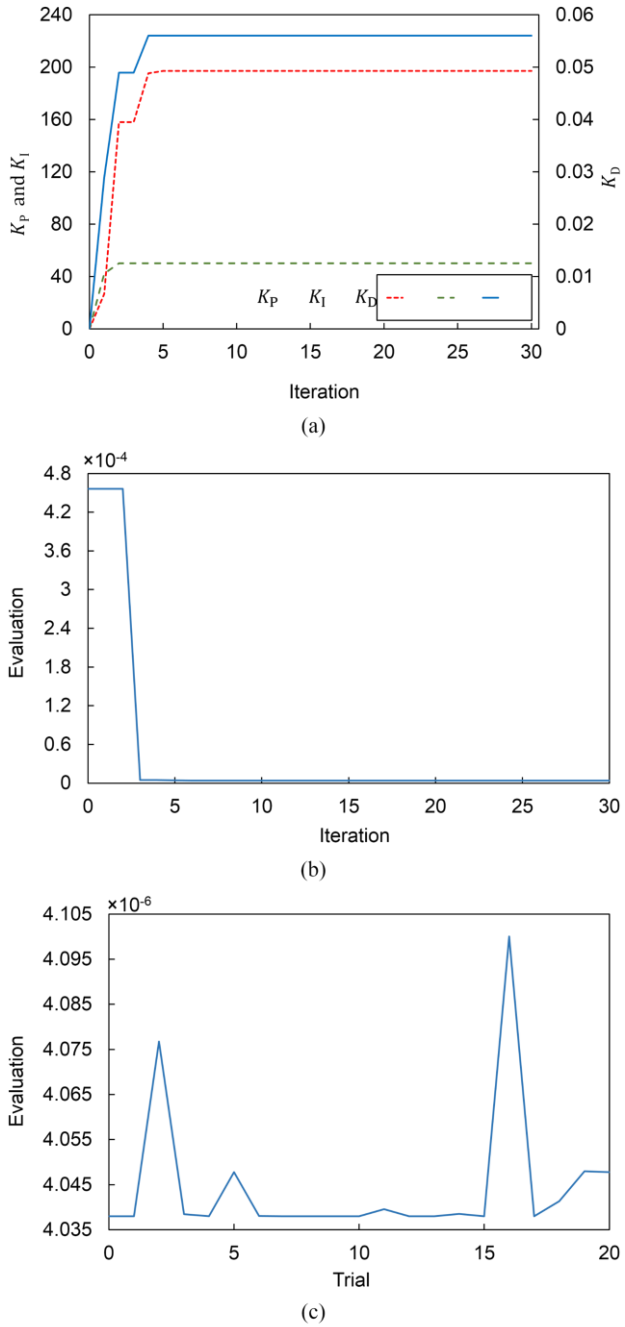

Fig. 5 PSO-based PID tuning results: (a) Convergence tendency of the optimal controller gains (δ = 2, population size = 30); (b) Convergence tendency of the of the evaluation value (δ = 2, population size = 30); (c) Fluctuation of the evaluation value (20 trials).

that those gains do not require many iterations to converge to their best solution, as shown in Fig. 5(a).

Thus, the minimum possible evaluation value could be achieved as fast as those gains reach to their best solution. This can be seen clearly in Fig. 5(b), which shows convergence tendency of the fourth simulation example. Observing Fig. 5(a and b), indicates that evaluation value starts to converge to its minimum value at the fifth iteration, which is the same iteration that the gains of the PID controller start to converge to their final values as well. As stated in Table 3, the fourth simulation example has the lowest standard deviation from its evaluation value, which makes it fluctuate in a small range when repeating the simulation for 20 trials to observe the repeatability of the solution. Fig. 5(c) presents the fluctuation manner of the fourth example when repeating the simulation for 20 trials, where the difference between the best (lowest) and the worst (highest) evaluation values is around 6.1992 ×10-7. This indicates that this simulation example has the best repeatability characteristics among the other examples. Thus, the best value of the weighting factor for the piezo-actuated system is 2, and the best gains for the PSO-based PID controller are those stated in the fourth example in Table 3.

The performance of the 2DOF controller when using the proposed fitness function is compared with the performance of the controller when using Integral Absolute Error (IAE) and Integral Time Squared Error ($ITSE$) as fitness functions. The results of such comparison are demonstrated in Fig. 6(a). It is clear that the proposed fitness function produces the best tracking control with a fast time response and zero overshoot.

The proposed fitness function is utilized to track the same triangular input voltage with the amplitude of 80 V and a frequency of 1 Hz, as in 2DOF tracking control. The 2DOF trajectory tracking control response is illustrated in Fig. 6(b), which shows that the displacement is almost relatively to the reference signal, with a considerably small error. The tracking error signal of the 2DOF controller is shown in Fig. 6(c). By comparing Fig. 6(c) and Fig. 4(b), it can be indicated that the error is significantly reduced to be in the range of -0.022 to 0.026 μm (0.030% of the maximum displacement) when the 2DOF controller was applied. This shows that the tracking performance is improved by 99.64%, as compared to the open-loop system. The hysteresis relationship between the input voltage and the displacement is demonstrated in Fig. 6(d), which shows that the relationship between the voltage and the displacement has become linear as the error is minimized.

To further investigate the performance of the proposed controller, the frequency (f) of the input signal is varied in the range of 1 – 50 Hz in several trials, while maintaining the same amplitude of 80 V. The performance is measured in terms of the maximum error ($e_{\max}$) and the root-mean-square error ($RMSE$), as summarized in Table 4. It can be seen that $e_{\max}$ and $RMSE$ are increasing according to the driving frequency. However, the proposed controller was able to limit $e_{\max}$ and $RMSE$ within 0.942 and 0.551 μm, respectively. Furthermore, the proposed controller shows better tracking performance when compared with previously reported control methods that use feedforward inverse hysteresis compensator along with different types of feedback controllers [3, 25-27].

Table 5 presents a comparison between these previously reported methods and the proposed controller in terms of the driving frequency, displacement range (Δy), maximum error, and the percentage error (e_p). The

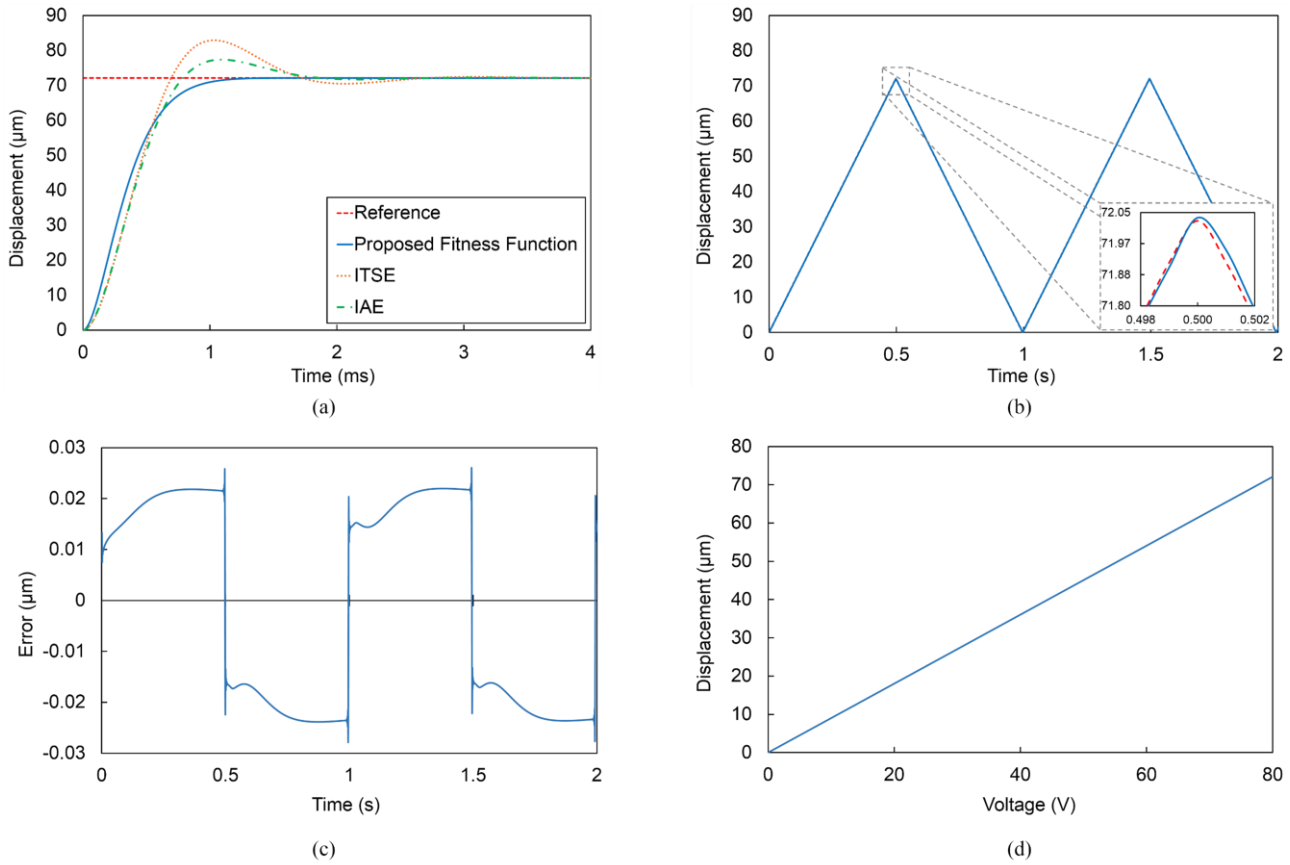

Fig. 6 2DOF control results: (a) trajectory tracking (step input); (b) Trajectory tracking with close-up view (triangular input); (c) Tracking error; (d) Hysteresis relationship.

Table 4 Tracking performance of the proposed controller with different frequencies

f (Hz)	e_{max} (μm)	*RMSE* (μm)
1	0.022	0.020
10	0.158	0.107
20	0.340	0.216
30	0.529	0.328
40	0.718	0.439
50	0.942	0.551

Table 5 Tracking performance of the proposed controller compared with previously reported control methods

Reference of method	f (Hz)	Δy (μm)	e_{max} (μm)	e_p (%)
[25]	0.2 Hz	40	0.5	1.250
[26]	0.2 Hz	40	0.11	0.275
[3]	1 Hz	34	0.612	1.80
[27]	1 – 5 Hz	30	0.05	0.167
Proposed method	1 – 50 Hz	72.02	0.022 – 0.942	0.03 – 1.31

table shows that the proposed control method is superior to the previously reported methods in term of the maximum displacement error while achieving a higher displacement range. This results in a lower percentage error, even when the system under study is operated at higher frequencies compared to the other systems. This proves the effectiveness of the designed 2DOF controller, which makes the system suitable to be used in high-precision positioning applications.

4. CONCLUSION

This paper has presented a novel design method for designing a 2DOF controller for precise positioning of a MEMS-based piezo-actuated stage. The piezo-actuated stage was modelled based on the Bouc-Wen hysteresis model. A 2DOF control approach of a piezo-actuated stage was designed for positioning control of the piezo-actuated stage. A Luenberger observer-based feedforward controller was designed and then combined with a PSO-based PID controller to form a 2DOF controller. Optimal PID gains were then obtained using a new fitness function proposed to reduce the displacement error and achieve a fast response time. The results showed that using the proposed 2DOF controller has reduced the hysteresis effect significantly, where the maximum error was minimized to 0.022 μm, which is about 0.030% of the maximum displacement (72.02 μm), while achieving a rise time and a settling time of 0.743 and 0.968 ms,

respectively. Additionally, the performance of the proposed controller was investigated in a frequency range of 1 – 50 Hz. The proposed controller was able to maintain a lower percentage error compared to previously reported control methods. Further improvement of this work can be done in the future using other optimization methods to tune the PID controller, such as radial basis function method [28] or metamodeling technique [29].

Acknowledgement

This work was supported by E-Science Fund (vote number-4S088) from Ministry of Science and Technology Malaysia and Innovation (MOSTI); and Fundamental Research Grant Scheme (vote number-4F646). Marwan Nafea acknowledges the financial support from the Malaysian Technical Cooperation Programme (MTCP).

References

[1] Yong-Sik, K., Jae-Myung, Y., Seung Ho, Y., Young-Man, C., Nicholas, G. D., and Satyandra, K. G. Design, fabrication and testing of a serial kinematic MEMS XY stage for multifinger manipulation. *Journal of Micromechanics and Microengineering.* Volume 22, (2012), p. 085029.

[2] Jingyan, D., Deepkishore, M., and Placid, M. F. Design, fabrication and testing of a silicon-on-insulator (SOI) MEMS parallel kinematics XY stage. *Journal of Micromechanics and Microengineering.* Volume 17, (2007), pp. 1154–1161.

[3] Zhenyan, W., Zhen, Z., and Jianqin, M. Precision tracking control of piezoelectric actuator based on bouc-wen hysteresis compensator. *Electronics letters.* Volume 48, (2012), pp. 1459-1460.

[4] Peng, J. and Chen, X. Novel models for one-sided hysteresis of piezoelectric actuators. *Mechatronics.* Volume 22, (2012), pp. 757-765.

[5] Lin, C.-J. and Yang, S.-R. Precise positioning of piezo-actuated stages using hysteresis-observer based control. *Mechatronics.* Volume 16, (2006), pp. 417-426.

[6] Yeh, T. J., Ruo-Feng, H., and Shin-Wen, L. An integrated physical model that characterizes creep and hysteresis in piezoelectric actuators. *Simulation Modelling Practice and Theory.* Volume 16, (2008), pp. 93-110.

[7] Zhao, X., Zhang, C., Liu, H., Zhang, G., and Li, K. Analysis of Hysteresis-Free Creep of the Stack Piezoelectric Actuator. *Mathematical Problems in Engineering.* Volume 2013, (2013), p. 10.

[8] Croft, D., Shed, G., and Devasia, S. Creep, hysteresis, and vibration compensation for piezoactuators: Atomic force microscopy application. *Journal of Dynamic Systems, Measurement, and Control.* Volume 123, (2001), pp. 35-43.

[9] Habibullah, H., Pota, H., Petersen, I. R., and Rana, M. Creep, Hysteresis, and Cross-Coupling Reduction in the High-Precision Positioning of the Piezoelectric Scanner Stage of an Atomic Force Microscope. *IEEE transactions on nanotechnology.* Volume 12, (2013), pp. 1125-1134.

[10] Gu, G. Y., Zhu, L. M., Su, C. Y., Ding, H., and Fatikow, S. Modeling and Control of Piezo-Actuated Nanopositioning Stages: A Survey. *IEEE Transactions on Automation Science and Engineering.* Volume 13, (2016), pp. 313-332.

[11] Zhu, W. and Wang, D.-h. Non-symmetrical Bouc–Wen model for piezoelectric ceramic actuators. *Sensors and Actuators A: Physical.* Volume 181, (2012), pp. 51-60.

[12] Qingsong, X. Enhanced discrete-time sliding mode strategy with application to piezoelectric actuator control. *IET Control Theory & Applications.* Volume 7, (2013), pp. 2153-2163.

[13] Devasia, S., Eleftheriou, E., and Moheimani, S. R. A survey of control issues in nanopositioning. *IEEE Transactions on Control Systems Technology.* Volume 15, (2007), pp. 802-823.

[14] Kennedy, J. and Eberhart, R. Particle swarm optimization. *Proceedings of the IEEE International Conference on Neural Networks.* Volume 4, (1995), pp. 1942-1948.

[15] Chiou, J.-S., Tsai, S.-H., and Liu, M.-T. A PSO-based adaptive fuzzy PID-controllers. *Simulation Modelling Practice and Theory.* Volume 26, (2012), pp. 49-59.

[16] Gu, G. and Zhu, L. High-speed tracking control of piezoelectric actuators using an ellipse-based hysteresis model. *Review of Scientific Instruments.* Volume 81, (2010), p. 085104.

[17] Lin, C.-Y. and Chang, C.-M. Hybrid proportional derivative/repetitive control for active vibration control of smart piezoelectric structures. *Journal of Vibration and Control.* Volume 19, (2013), pp. 992-1003.

[18] Xie, H., Liu, Z., Yang, J., Sheng, Z., and Xu, Z. Modelling of magnetorheological damper for intelligent bionic leg and simulation of knee joint movement control. *International Journal of Simulation Modelling.* Volume 15, (2016), pp. 144-156.

[19] Luenberger, D. An introduction to observers. *IEEE Transactions on Automatic Control.* Volume 16, (1971), pp. 596-602.

[20] Gaing, Z.-L. A particle swarm optimization approach for optimum design of PID controller in AVR system. *IEEE Transactions on Energy Conversion.* Volume 19, (2004), pp. 384-391.

[21] Eberhart, R. C. and Yuhui, S. Particle swarm optimization: developments, applications and resources. *Proceedings of the 2001 Congress on*

Evolutionary Computation. Volume 1, (2001), pp. 81-86.

[22] Nafea, M., Kazi, S., Mohamed, Z., and Mohamed Ali, M. S. A hybrid control approach for precise positioning of a piezo-actuated stage. *2014 14th International Conference on Control, Automation and Systems (ICCAS)* Volume, (2014), pp. 667-671.

[23] Nafea, M., Mohamed, Z., Abdullahi, A. M., Ahmad, M. R., and Husain, A. R. Dynamic hysteresis based modeling of piezoelectric actuators. *Jurnal Teknologi (Sciences and Engineering).* Volume 67, (2014), pp. 9-13.

[24] Lin, C.-Y. and Tsao, T.-C. Adaptive Control With Internal Model for High-Performance Precision Motion Control and Its Application to a Fast-Acting Piezoelectric Actuator. *Journal of Dynamic Systems, Measurement, and Control.* Volume 135, (2013), pp. 061012-061012.

[25] Li, Y. and Xu, Q. Adaptive sliding mode control with perturbation estimation and PID sliding surface for motion tracking of a piezo-driven micromanipulator. *IEEE Transactions on Control Systems Technology*. Volume 18, (2010), pp. 798-810.

[26] Yangmin, L. and Qingsong, X. A Novel Piezoactuated XY Stage With Parallel, Decoupled, and Stacked Flexure Structure for Micro-/Nanopositioning. *IEEE Transactions on Industrial Electronics.* Volume 58, (2011), pp. 3601-3615.

[27] Xiao, S. and Li, Y. Dynamic compensation and control for piezoelectric actuators based on the inverse Bouc–Wen model. *Robotics and Computer-Integrated Manufacturing.* Volume 30, (2014), pp. 47-54.

[28] Mohamed Ali, M. S., Abdullah, S. S., and Osman, D. C. Controllers optimization for a fluid mixing system using metamodeling approach. *International Journal of Simulation Modelling.* Volume 8, (2009), pp. 48-59.

[29] Malek, M. N. and Mohamed Ali, M. S. Evolutionary tuning method for PID controller parameters of a cruise control system using metamodeling. *Modelling and Simulation in Engineering.* Volume 2009, (2009), pp. 9-16.